

## APPLICATION OF DISCRETE ELEMENT METHOD IN GRINDING MILLS AND COMPOSITE PARTICLE BREAKAGE

CHANDANA T. JAYASUNDARA<sup>1</sup>, MANOJ KHANAL<sup>1</sup>, AND DEEPAK ADHIKARY<sup>1</sup>

<sup>1</sup>Commonwealth Scientific and Industrial Research Organization, CSIRO  
Queensland Centre for Advanced Technologies, 1 Technology Court  
Pullenvale, QLD 4069, Australia.

*Corresponding author: Manoj Khanal (manoj.khanal@csiro.au)*

**ABSTRACT.** In particle industries, Discrete Element Modeling (DEM) is one of the frequently used numerical tools to analyze free flow, processing, fracture and fragmentation behavior of particles and to get insight into the mechanism involved in processing of them. DEM also has wide spread application in various engineering disciplines and communities to understand the failure behavior of heterogeneous structures. DEM treats the specimen as constituents of different individual primary particles which are governed by laws of motion and material constitutive behavior. Compared to continuum models, the DEM needs to specify micromechanical properties and contact parameters such as stiffness and bond strength. The paper discusses the applications of DEM in particle processing in various milling operations and shows linkage between micro-dynamic properties obtained from DEM and grinding performances. Further, the paper also deals with the application of DEM simulation to investigate fracture and fragmentation mechanism of composite heterogeneous particles under various loading conditions.

**Keywords.** Discrete element method, Grinding, Comminution

**AMS (MOS) Subject Classification.** 65N99, 74S30.

### 1. Introduction

In Discrete Element Method (DEM) particles are considered to be distinct elements. The laws of motion and material constitutive laws are applied to each element. Two types of discrete element modelling approaches: soft particle and hard particle are common in particle processing. The soft-sphere method was originally developed by Cundall and Strack (1979). In this approach, particles are allowed to have an overlap, and these deformations are used to calculate elastic and frictional forces between particles. The motion of particles is described by the well established Newton's laws of motion. Soft-sphere models are capable of handling multiple particle contacts which are of importance when modelling quasi-static systems. On the other hand in hard-particle approach, often the forces between particles are not explicitly considered. Both methods, particularly the soft-sphere method, have been extensively used

to study various phenomena, such as particle packing, transport properties, heaping/piling process, hopper flow, mixing granulation, fragment and fragmentation and recycling of materials (Schubert et al 2005; Zhu et al 2007).

The proposed paper discusses the use of DEM in application to milling of discrete particles and breakage of a composite particle. The DEM results are compared with the experimental observations in order to calibrate and validate the models. An attempt has been made to investigate relationship between micro-dynamic properties and grinding kinetics. The paper also shows an application of DEM to capture the fragmentation mechanisms of heterogeneous and anisotropic composite particles.

**1.1. Governing Equations and Force Models.** A particle in a granular flow can have two types of motion: translational and rotational. During its movement, the particle may interact with its neighbouring particles or walls. In DEM approach, it is generally assumed that this problem can be solved by choosing a numerical time step less than a critical value so that during a single time step the disturbance cannot propagate from the particle farther than its immediate neighbouring particles (Cundall and Strack, 1979). Thus, at all times the resultant forces on a particle can be determined exclusively from its interaction with the contacting particles. For a fine particle system, non-contact forces such as the van der Waals and electrostatic forces should also be included. Based on these considerations, Newton's second law of motion can be used to describe the motion of individual particles. It calculates the new velocities and displacements from stresses and forces with an explicit time stepping scheme. Using suitable material constitutive behaviour, new stresses and displacements are calculated for each element. The governing equations for the translational and rotational motion of particle  $i$  with mass  $m_i$  and moment of inertia  $I_i$  can be written as

$$(1.1) \quad m_i \frac{d\mathbf{v}_i}{dt} = \sum (\mathbf{F}_{ij}^n + \mathbf{F}_{ij}^s + m_i \mathbf{g})$$

and

$$(1.2) \quad I_i \frac{d\boldsymbol{\omega}_i}{dt} = \sum (\mathbf{R}_i \times \mathbf{F}_{ij}^s - \mu_r R_i |\mathbf{F}_{ij}^n| \hat{\boldsymbol{\omega}}_i)$$

where  $\mathbf{v}_i$ ,  $\boldsymbol{\omega}$ , and  $I_i$  are, the translational velocity, angular velocity and moment of inertia of the particle, respectively, while  $\hat{\boldsymbol{\omega}}_i$  represents a unit vector equal to  $\boldsymbol{\omega}_i$  divided by its magnitude.  $\mathbf{R}_i$  is a vector running from the centre of the particle to the contact point with its magnitude equal to particle radius  $R_i$ .  $\mathbf{F}_{ij}^n$  and  $\mathbf{F}_{ij}^s$  represent, respectively, the normal contact force and the tangential contact force imposed on particle  $i$  by particle  $j$  and  $m_i \mathbf{g}$  is the gravitational force. The first part of the right side in Eq. (1.2) is the torque caused by tangential force  $\mathbf{F}_{ij}^s$  and the second part is

the rolling friction torque caused by normal force  $F_{ij}^n$ , where  $\mu_r$  is the coefficient of rolling friction.

**1.2. Contact Models.** Several methods (linear spring mass, Hertz, Hertz-Mindlin, JKR) are reported in literatures to model contact dynamics and calculate contact forces from the neighbouring particles. The selection of the contact model for a particular analysis depends on the constitutive behaviour of the particles, objective of the specific simulation, assumptions, accuracy and detail required in analysis. Mostly, two major types of contact models are widely used in DEM simulations to model free flow of particles. The first one is a ‘simplified’ approach that uses a conventional linear spring dashpot slider model to represent particle interactions. The second one is based on contact mechanics and generic interactions are derived from Hertz–Mindlin principles, which is a non-linear approach in modelling particle contacts. Hertz (1881) proposed a theory to describe the elastic contact between two spheres in the normal direction. He considered that the relationship between the normal force and normal displacement was nonlinear. Mindlin and Deresiewicz (1953) proposed a general tangential force model. Recently, some researchers have applied a combination of both approaches to represent particle interactions.

*Linear Contact Model.* Figure 1 shows the linear (force/displacement) spring mass contact model which is the simplest model and widely used in simulating particle interactions. The linear contact model is defined in terms of the normal and tangential stiffnesses that exist between two contacting entities. The normal contact force results from the sum of an elastic spring force and a damping force. The tangential contact force considers additionally the friction at the contact between the particles. where  $k_{c,ij,n}$  is the contact stiffness in normal direction;  $k_{c,ij,s}$  the contact stiffness in shear direction;  $s_{ij,n}$  the overlap between two particles in normal direction,  $s_{ij,s}$  the overlap in shear direction,  $a$  the constant ( $a = 1$ , Hooks law and  $a = 1.5$ , Hertz contact law),  $\eta_{ij}$  the damping coefficient, and  $\mu_{ij}$  is the dynamic friction coefficient. The unit vector  $n_{ij}$  is directed outward from particle  $i$  and is normal to the contact surface of the partners and perpendicular to the unit tangential vector  $t_{ij}$ .

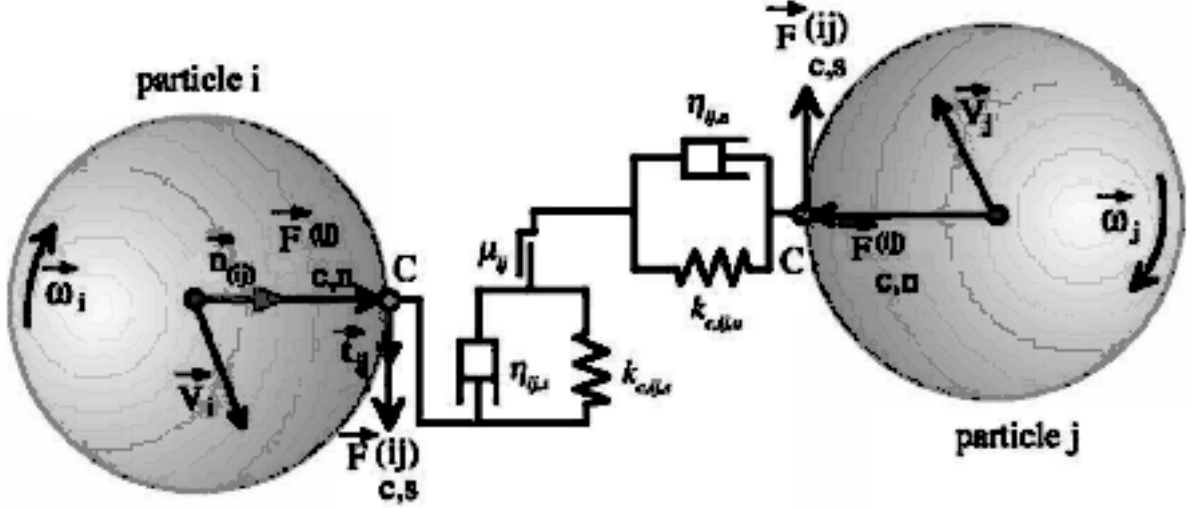


Figure 1. Linear Contact laws (linear spring mass model) (Antonyuk et al, 2006).

Normal force

$$\vec{F}_{c,n}^{(ij)} = (k_{c,ij,n} s_{ij,n}^a + \eta_{ij,n} \dot{s}_{ij,n}) \vec{n}_{ij}$$

Shear force

$$\vec{F}_{c,s}^{(ij)} = \min \left| \begin{array}{l} (k_{c,ij,s} s_{ij,s}^a + \eta_{ij,s} \dot{s}_{ij,s}) \vec{t}_{ij} \\ (\mu_{ij} F_{c,n}^{(ij)}) \vec{t}_{ij} \end{array} \right|$$

*Simplified Hertz–Mindlin and Deresiewicz model.* In simplified Hertz–Mindlin and Deresiewicz model, the contact forces are given by,

$$(1.3) \quad F_{ij}^n = \left[ \frac{2}{3} E \sqrt{R} \xi_n^{\frac{3}{2}} - \gamma_n E \sqrt{R} \sqrt{\xi_n} (v_{ij} \cdot \hat{n}_{ij}) \right] \hat{n}_{ij}$$

and

$$(1.4) \quad F_{ij}^s = -\text{sgn}(\xi_s) \mu |F_{ij}^n| \left[ 1 - (1 - \min(\xi_s, \xi_{s,\max}) / \xi_{s,\max})^{3/2} \right] \hat{\xi}_s$$

where  $E = Y / (1 - \tilde{\sigma}^2)$ , and  $Y$  and  $\tilde{\sigma}$  are, respectively, Young's modulus and Poisson ratio;  $\xi_n$  is the overlap between particles  $i$  and  $j$ ;  $\hat{n}_{ij}$  is a unit vector running from the centre of particle  $j$  to the centre of particle  $i$ ;  $\bar{R} = R/2$  for mono-sized particle. The normal damping constant,  $\gamma_n$ , is the material property directly linked to the coefficient of restitution  $e$ .  $\xi_s$  and  $\xi_{s,\max}$  are, the total and maximum tangential displacements of particles during contact respectively.  $\hat{\xi}_s$  is the unit vector of  $\xi_s$ .

*Solid bridge bonds.* Similarly, fragmentation of particles can be studied using solid bridge bonds, as show in Figure 2. In this case, the neighbouring particles are bonded with physically strong contact bonds, solid bridge bonds, and are more or less a kind of a solid state bond between the particles. It describes the constitutive behaviour of a finite-sized piece of cementitious material deposited between two particles. Both normal and shear forces as well as moments are transmitted by the solid bridge

bonds where as only normal and tangential forces are transmitted by linear spring mass contact model. In simple, solid bridge bonds can be interpreted as a number of linear spring contacts joined in parallel between pair of particles with constant normal and shear stiffnesses uniformly distributed over a contact cross section. The equivalent stiffness of the set of springs in normal direction can be represented by a right hand side picture of Figure 2 and is evaluated by equation (1.5). The similar equation can be derived for the shear direction. In equation (1.5),  $k_{b,m,n}$  is the stiffness related to solid bridge bond in normal direction with the cross-section area of  $A_{ij}$ . Equations (1.6) and (1.7) represent the normal and shear forces, respectively, acting on the particles.

$$(1.5) \quad k_{equiv,n} = \left( \frac{1}{k_{c,i,n}} + \frac{1}{k_{c,j,n}} \right)^{-1} + k_{b,m,n} A_{ij}$$

Normal force

$$(1.6) \quad \vec{F}_{b,n}^{(ij)} = (k_{b,m,n} A_{ij} s_{ij,n}) \vec{n}_{ij}$$

Shear force

$$(1.7) \quad \vec{F}_{b,s}^{(ij)} = (k_{b,m,s} A_{ij} s_{ij,s}) \vec{t}_{ij}$$

The moment in cross-section area can be expressed as:

$$(1.8) \quad M_b^{(ij)} = k_{b,m,n} I_b^{(ij)} \Delta \varphi_{ij}$$

Where  $I_b$  is the moment of inertia of the circular bond cross-section about an axis of symmetry. The increment of the rotation angle  $\varphi_{ij}$  between two particles is given by:

$$(1.9) \quad \Delta \varphi_{ij} = (\omega_i - \omega_j) \Delta t$$

Where  $\omega$  is the angular velocity of the particle.

The relative motion at the contact (with solid bridge bond) causes a force and a moment to develop within the bond material as a result of the solid bridge bond stiffness. This force and moment acting on the two bonded particles (i and j) can be reduced to the normal ( $\sigma_{ij}$ ) and shear ( $\tau_{ij}$ ) stresses acting within the cross-section of a solid bridge bond. If either of these stresses reaches its corresponding bond strength ( $\sigma_{b,max}$  and  $\tau_{b,max}$ ) the solid bond breaks (PFC, 2002). Due to this mechanism, the modelling allows to study the crack simulations of composite particles.

$$(1.10) \quad \sigma_{ij} = \frac{-F_{b,n}^{(ij)}}{A_{ij}} + \frac{|M_b^{(ij)}|}{I_b^{(ij)}} R_b^{(ij)} = \sigma_{b,\max}$$

$$(1.11) \quad \tau_{ij} = \frac{|F_{b,n}^{(ij)}|}{A_{ij}} = \tau_{b,\max}$$

$R_b$  is the radius of the bond cross-section

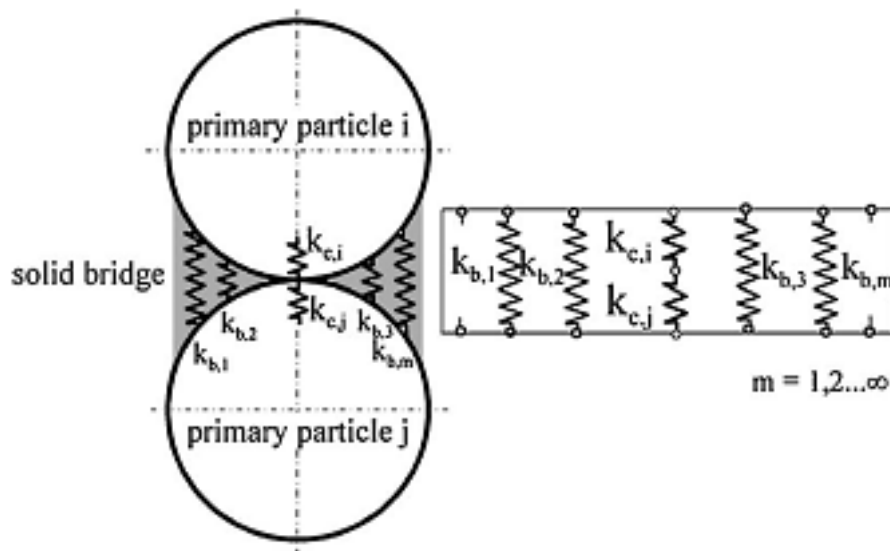


Figure 2. Representation of solid bridge bonds (Antonyuk et al, 2006).

*Comparison between linear contact model, and Simplified Hertz–Mindlin and Deresiewicz model.* The effect of linear and non-linear contact model on normal impact of particle can be exhibited with the following DEM simulation. A single particle of diameter 15mm was dropped from a height of 50mm on to a flat surface under gravity. Figure 3 shows the contact force–displacement relationship for linear and Hertz contact models with the identical particle properties. The linear model is relatively straight forward, whereas due to the nonlinear Hertz contact model, the particle shows a nonlinear force displacement behaviour. Nonlinear Hertz model allows the Young’s modulus to vary according to a second order polynomial function of the inter-particle overlap because one would expect the contact area between the colliding structures to increase as the contact force increases, leading to a non-linear stiffness described by the Hertz coefficient.

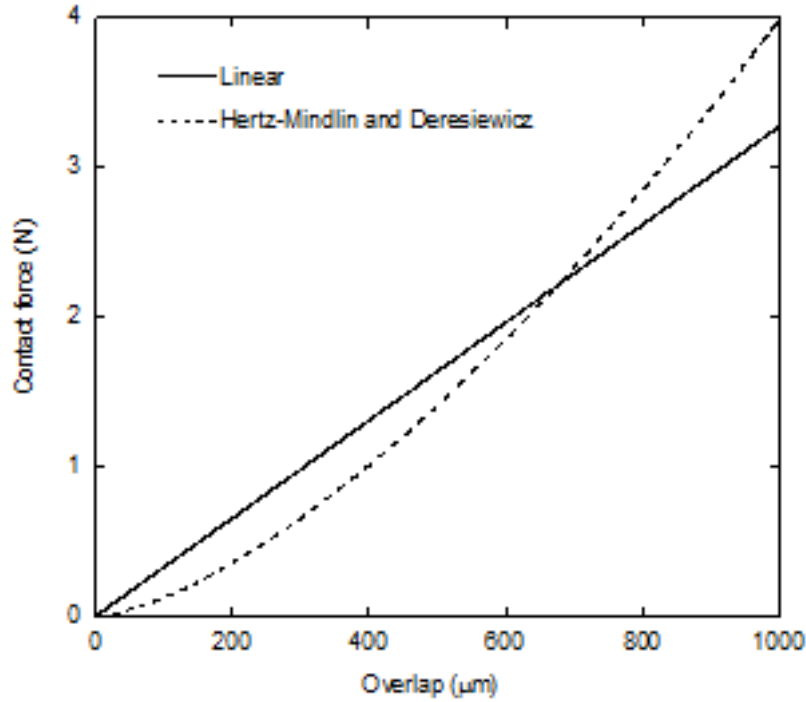


Figure 3. Comparison between linear and Simplified Hertz–Mindlin and Deresiewicz model.

1.3. **Time Step.** To ensure the stability and accuracy of the numerical simulation a suitable value for the time step  $\Delta t$  has to be chosen. The critical time step corresponding to a second order finite difference scheme for the simple mass spring system of point mass  $m$ , and spring stiffness  $k$ , and the motion of which is governed by differential equation  $m\ddot{s} = -ks$  is given by

$$(1.12) \quad t_{crit} = \frac{T}{\pi}$$

$$(1.13) \quad T = 2\pi\sqrt{\frac{m}{k}}$$

Where,  $T$  is the period of the system,  $m$  is the weighted mass with the same stiffness. It is determined on the basis of the maximum stiffness and the particle with smallest mass. The critical time step can be found to be:

$$(1.14) \quad t_{crit} = C\sqrt{\frac{m}{4k}} = \sqrt{\frac{m}{k^{tran}}} \quad \text{for translation motion}$$

$$(1.15) \quad t_{crit} = \sqrt{\frac{I}{k^{rot}}} \quad \text{for rotational motion}$$

Different values have been proposed for the constant  $C$  in the literature. For example 0.1 (Thompson & Grest, 1991; Zhang & Campbell, 1992) and 2 (Yuu et al.,

1995; Rajamani et al., 2000). Trial runs are normally conducted to evaluate the most appropriate time step to be used. If the time step is too small several drawbacks can be identified such as propagation of rounding errors, artificial oscillations, and unnecessarily long runtimes. In this model,  $c=2$  has been chosen.

**1.4. Calibration.** One of the challenges in the DEM modelling is to calibrate and validate the micro-mechanical model. Mostly process parameters associated with experimental results or time dependent observations are used to calibrate the model. Due to the micro properties, which are not exactly known from the macro properties, and to match the known behaviour from the observation is a time consuming and complicated process, hence it is an iterative process and may take a significant amount of the modelling time. For the free particles in milling operations, the calibration can be performed from the experimental data. In this case, in order to calibrate the DEM model, experiments have been conducted with stirred and ball mills. As an example power draw has been selected to calibrate the model. Figure 4 shows experimental and simulation power comparison for a stirred mill operating at mill loading 40% and different mill speeds. The curves show the increase in power consumption with the increase in mill speed.

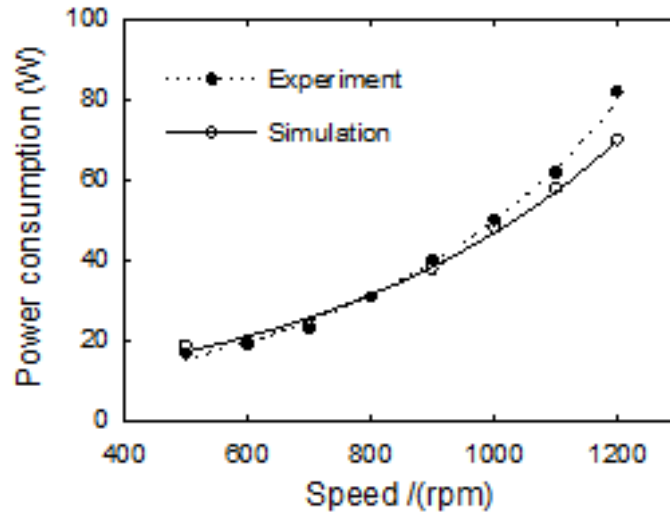


Figure 4. Experimental and simulation power consumption for the stirred mill.

Furthermore, simulations have been carried out in ball mills with identical geometry and operating conditions as used in the literature (Malghan, 1976). Mill diameters are 127mm, 254mm and 508mm where mill length to diameter ratio is 1.15. Each mill consists of eight lifters which have the same dimensions. Steel balls of 25.4mm diameter have been used as the grinding media. Figure 5 shows the experimental and simulation power comparison for different size of ball mills. A good agreement between experimental and simulated mill power consumptions can be observed. This

type of close match between the experiments and the DEM shows the confidence in selected parameters.

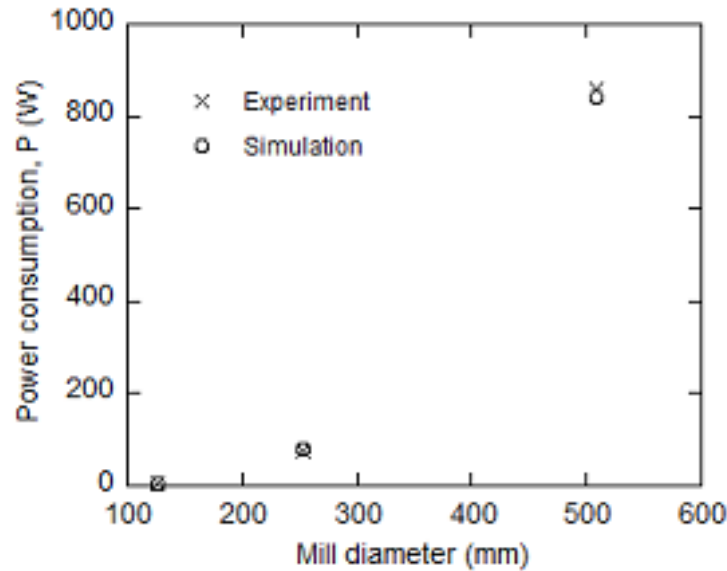


Figure 5. Experimental and simulation power consumption for different size of ball mills.

## 2. Applications

Grinding is a common process in mineral industry. It is known as a low-efficiency (<10 %, typically), power-intensive process and may account for up to 40% of the direct operating cost of a mineral processing plant (Prasher, 1987; Wills, B.A., 1992). Most commonly used grinding mills can be categorized as ball and stirred mills. Ball mills are used for coarse grinding whereas stirred mills are used for fine and ultra-fine grinding.

Despite gaining increasingly industrial importance, most of the grinding mill studies have been done based on experience and trial and error tests, rather than the detailed scientific principles. Since the bulk behaviour of flow depends on the collected outcome of the interactions between particles and between particles and mill, a better understanding of the flow at an individual particle level would facilitate the improvement of mill performance. However, obtaining such microscopic information is a very difficult, if not impossible, task using conventional experimental techniques.

To overcome above mentioned difficulties, numerical models based on the DEM can be used to study particle flow in grinding mills (Mishra B.K, 2003). The DEM results can be used to obtain spatial distributions of microdynamic variables related to flow and force structures such as local porosity and particle interaction forces, collision velocity and collision frequency in different regions of the mill (Khanal and Morrison 2008; Jayasundara et al., 2006). Moreover, it was shown that microscopic

information obtained from DEM can be linked with the grinding performance (Kano et al, 2000; Jayasundara et al, 2010).

*Mill characteristics analysis.* Figure 6 shows the particle flow pattern for the stirred mill. At the low loading  $J = 40\%$ , most particles stay at the bottom with slow movement and only a small number of particles are agitated by the rotating discs to the upper part of the mill.

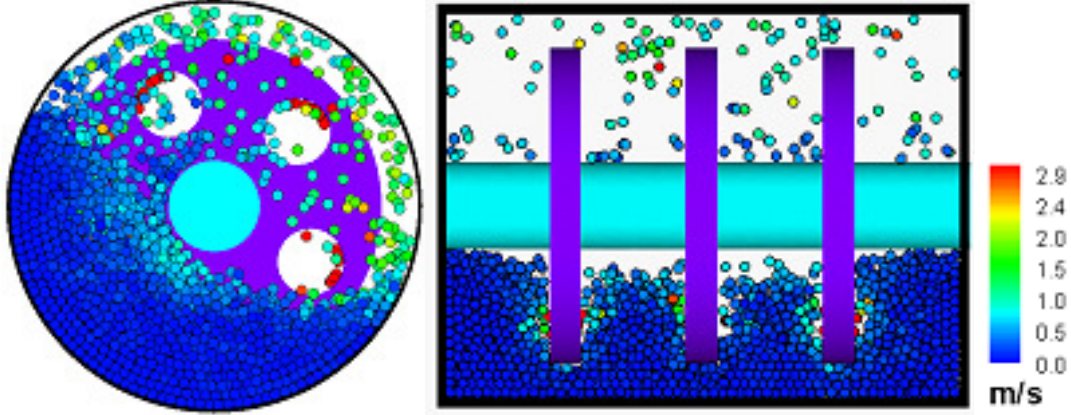


Figure 6. Particle flows in the radial (section  $YY'$ ) and axial (section  $XX'$ ) directions for  $J = 40\%$ ; and  $\Omega = 1200$  rpm.

*Grinding rate and impact energy analysis.* While DEM modelling is able to simulate particle flow and provide a significant amount of information at the particle scale, currently it is still difficult to simulate particle breakage directly in a grinding process due to the limited computational capability. Therefore, establishing a quantitative link between the microscopic DEM results and grinding performance can provide a way of predicting and optimise the grinding processes based on simulation results (Khanal and Morrison, 2008).

Based on the simulation and experimental results it was observed that the grinding rate has a linear correlation with the impact energy among particles. The results showed that the change of particle size with grinding time follows the first-order kinetics, given by

$$(2.1) \quad \frac{D_t - D_\infty}{D_0 - D_\infty} = \exp^{-K_p t}$$

where  $D_0$ ,  $D_t$ , and  $D_\infty$  are the original particle size, particle size at grinding time  $t$  and the limiting size after an infinite grinding time, respectively;  $K_p$  is the grinding rate constant (Jayasundara et al, 2010).

Figure 7 shows the cumulative size distribution of the ground samples measured at different times when  $J = 40\%$  and  $\Omega = 800$  rpm. Similar distributions are also obtained for other mill loadings and speeds. The distribution curves shift continuously

towards the finer side as the grinding progresses. Consistent with the normal practice, 80% passing particle size  $D_{80}$  was selected to represent the particle size in order to quantitatively investigate grinding performance under different conditions. The log-linear plots of  $\frac{(D_t - D_\infty)}{(D_0 - D_\infty)}$  and grinding time  $t$  in Fig. 8 show straight lines for all cases, although different slopes are observed for different mill speeds. This indicates that the grinding process follows the first-order kinetics, and the particle size decays exponentially with time as described in Eq. 16. The grinding rate constant  $K_p$  (line slope) obtained from Figure 8 shows an increase with mill speed.

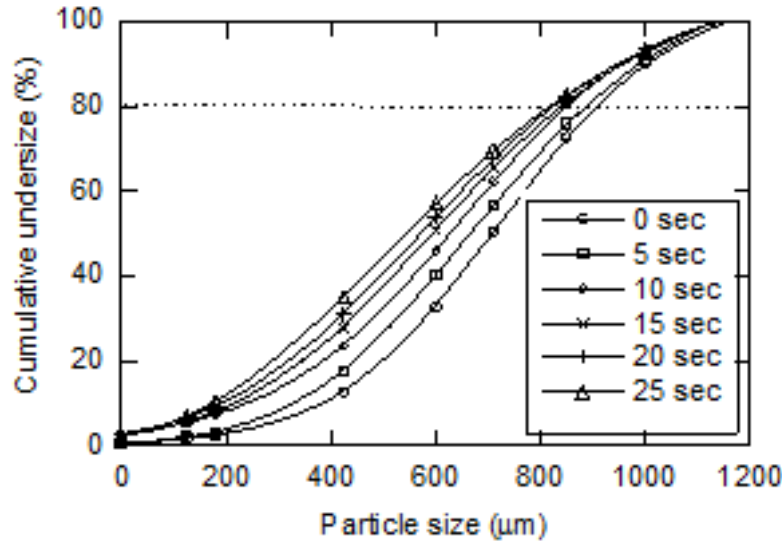


Figure 7. Cumulative particle size distribution at different times when  $J = 40\%$  and  $\Omega = 800\text{rpm}$ .

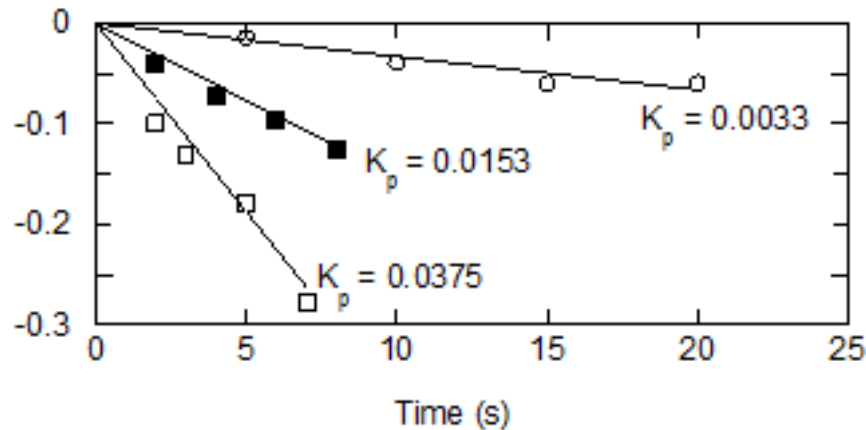


Figure 8. Normalized particle size of the ground sample as a function of grinding time for different mill speeds ( $\circ$ , 400rpm;  $\blacksquare$ , 800rpm; and  $\square$ , 1000rpm) when  $J=60\%$ .

Figure 9 represents the relationship between  $K_p$  and  $E_i$  obtained at different mill loadings and speeds using  $D_{80}$  and  $D_{50}$  to represent the particle size. Here,  $E_i$  is the total impact energy per unit time. Impact energy is given by  $\frac{1}{2}m_i v_{ij}^2$ , where  $m_i$  is the

mass of a particle and  $v_{ij}$  ( $= |v_i - v_j|$ ) is the relative collision velocity between two particles. Both curves show that  $K_p$  increases with  $E_i$ . Notably, all the data falls into a single curve which can be fitted by a power law. For different ground materials, the  $K_p \sim E_i$  curves may change depending on their properties. The present results confirm that impact energy is a very useful parameter to describe the grinding performance of mills. The results also demonstrate that the DEM based microscopic study can be linked to macroscopic process performance. Therefore, numerical simulations can be carried out to understand the actual grinding behaviour in milling processes. With fast advancement of computing capability, this technique has potential to reduce laborious experiments. To achieve this, however, more systematic studies are necessary in order to generalize this approach.

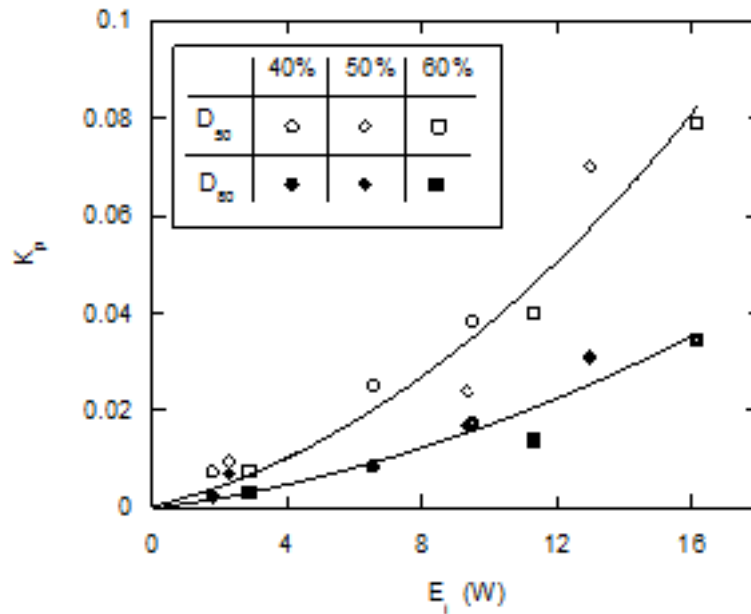


Figure 9. Correlation between grinding rate constant and total impact energy for  $D_{80}$  and  $D_{50}$  passing sizes.

*Particle position and energy analysis.* DEM are widely used to understand and characterize the milling and crusher performances in various industries. Left and right pictures in Figure 10 shows the snapshot of position of particles at steady state condition inside the mill and the velocity distribution of particles in the rotating mill. The velocity distribution has been extracted along the XX' line. At 70% of mill critical speed the maximum velocity of the particles in the mill is around 5m/s which is achieved by only few particles due to free fall from the top of the mill. Whereas at the centre of the milling zone, the particle velocities are in the range of less than 1m/s. As observed in most of the experimental observations, from Figure 10 (left) it can be inferred that particles grind/fail due to rolling and grinding mechanisms at the centre

of the milling zone and at the boundary of the milling zone particles fail due to free fall of particles.

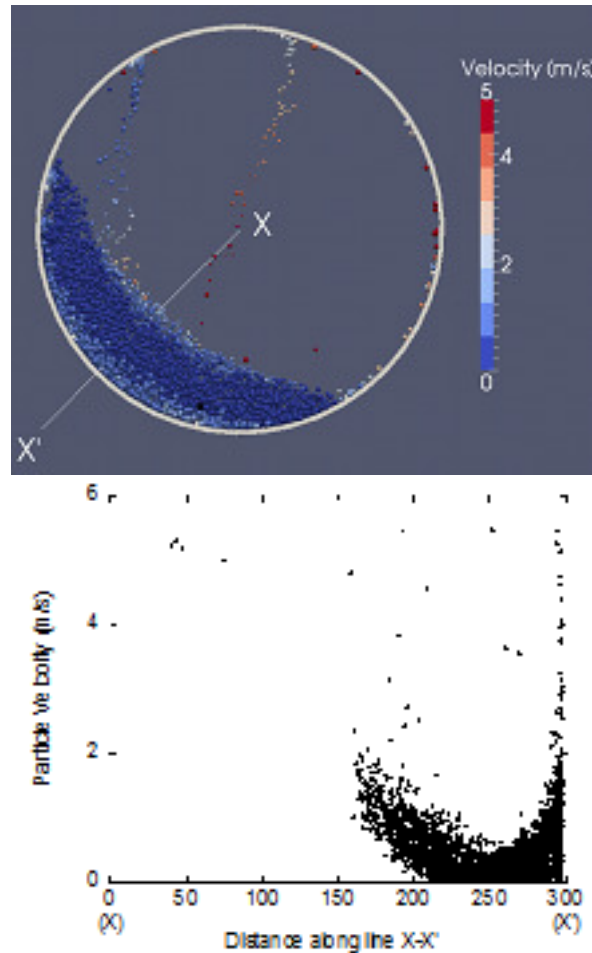


Figure 10. Snapshot of position of particles at steady state condition inside the mill (left) and velocity distribution of particles along the cross-section XX' (right).

Similarly, Figure 11 shows the release height of the particles versus time for 1.1 and 0.6m mills with 36 particles (Khanal and Morrison, 2008). The average release height for 1.1m and 0.6m mills with 36 particles is 0.94m and 0.52m in simulations and 0.97m and 0.54m in experiments (see Khanal and Morrison, 2008) respectively. The release height was calculated from the difference in position of the particles (along the height of the mill) in one revolution of the mill. The slight difference in the release height is due to the selection of particles to trace the height in experiments and simulations. DEM simulations can also be used to investigate the energy utilization in the processing equipment. Figure 12 shows the energy utilization during collision for 1.1 and 0.6m mills with 36 particles of equal masses at the same rpm and lifters. The larger mill requires more energy to start the mill than the smaller mill. Due to the equal mass of the particles in each mill, the steady state energy utilization is very close to each other in both the mills.

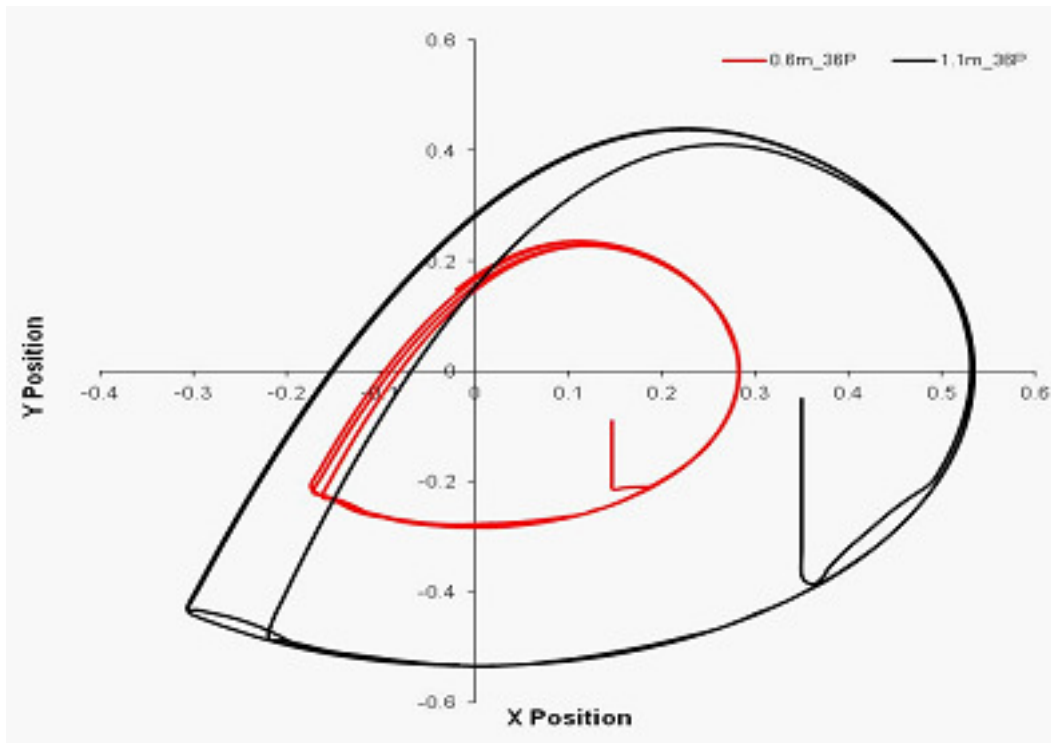


Figure 11. Simulated release heights for different mills (Khanal and Morrison, 2008).

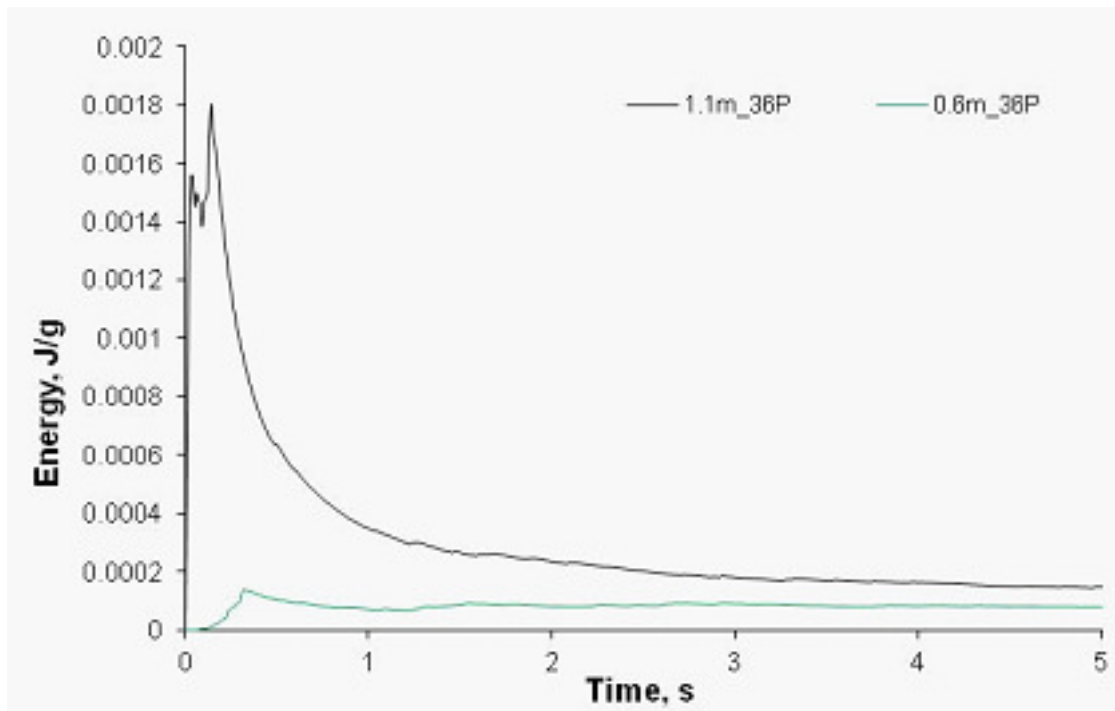


Figure 12. Energy utilization during collision for 1.1 and 0.6m mills with 36 particles of equal masses at the same rpm and lifters.

*Composite particle fragmentation analysis.* DEM are well suited tool to explore the fragmentation of composite particles. Depending on the applications, the composite particles are fragmented to either extract valuable minerals from the cheap matrices

or for further applications. In DEM composite particles are created by combining numerous primary particles, as shown in Figure 13. The larger primary particles represent valuable aggregates present within the cheaper matrices represented by smaller particles.

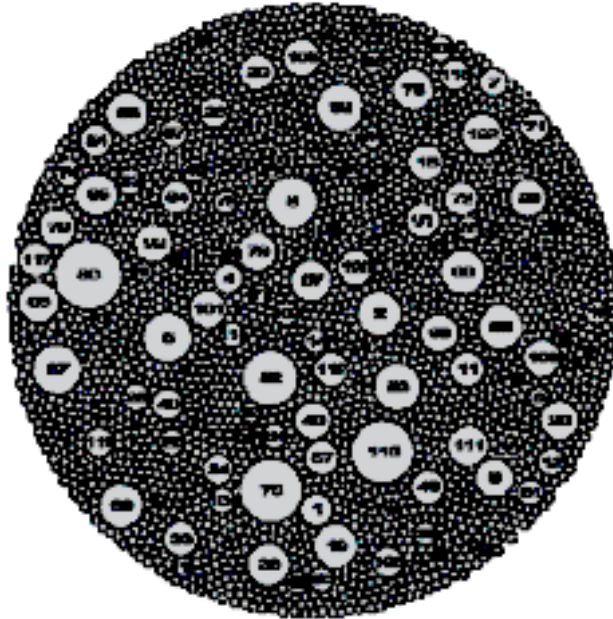


Figure 13. Tentative arrangement of aggregates and hardened cement paste (Schubert et al, 2005).

DEM can be used to analyse energy utilization and failure phenomena of particles for high speed velocity and high loading rate dependent events, which is very difficult to capture during experiments (Khanal et al, 2005; Khanal and Tomas, 2009). For example, Figure 14 shows different impact events during central impact of the agglomerate at a velocity of 7.7 m/s. The specimen undergoes contact deformation as it touches the target wall and then the crack initiates. It can be noticed from these different stages that once the cracks have been initiated, they propagate between the primary particles.

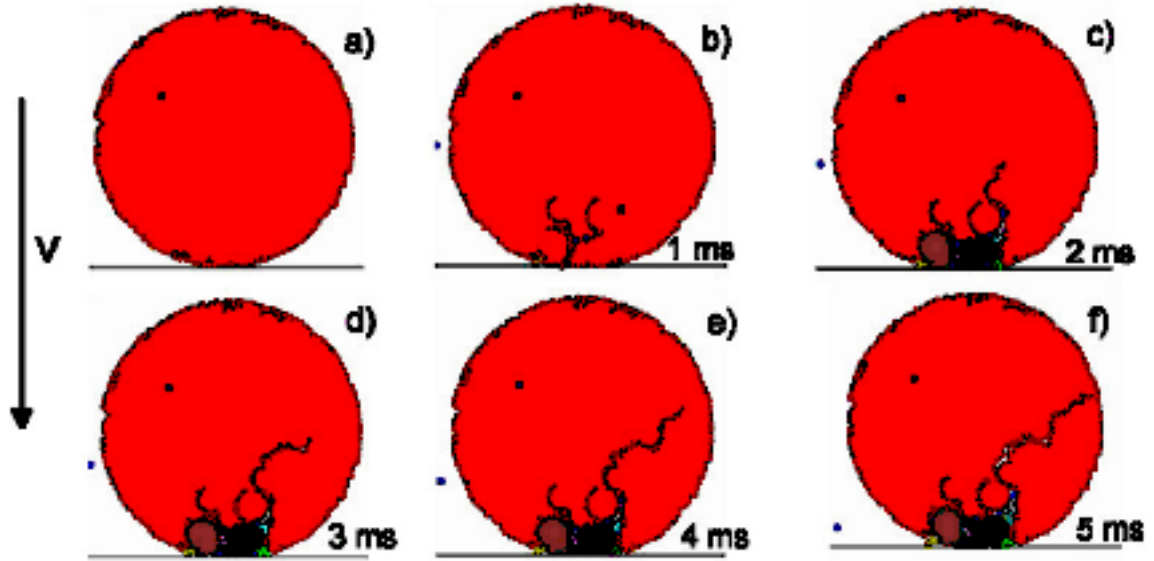


Figure 14. Impact stages at an impact velocity of 7.7m/s (Khanal and Tomas, 2009).

### 3. Conclusions

The paper discussed the applications of DEM in grinding mills and composite particle breakage. It has been shown that the various particle processing parameters can be evaluated using DEM. The results indicate that the total impact energy obtained from particle scale simulation, can be a useful index to predict grinding performance. It has also been shown that the micro failure of composite particles can also be studied using DEM.

### ACKNOWLEDGMENTS

The authors would like to thank to anonymous referee for the valuable suggestions.

### REFERENCES

- [1] Antonyuk, S., Khanal, M., Tomas, J., Heinrich, S., Moerl, L., Impact breakage of spherical granules: Experimental study and DEM simulation, *Chemical Engineering and Processing* 45, 838–856, 2006.
- [2] Cundall, P. A., and Strack, O. D. L. A discrete numerical model for granular assemblies. *Geotechniques*, 29, 47, 1979.
- [3] Hertz, H., On the contact of elastic solids. *Journal fur die reine und angewandte Mathematik*, 92, 156-171, 1881.
- [4] Khanal, M., Morrison, R., Discrete element method study of abrasion, *Minerals Engineering*, 21, 751–760, 2008
- [5] Khanal, M., Schubert, W., Tomas, J., DEM simulation of diametrical compression test on particle compounds, *Granular Matter*, 7 (2-3), 83-90, 2005.

- [6] Khanal, M., Tomas, J., Oblique impact simulations of high strength agglomerates, *Advanced Powder Technology*, 20, 150–157, 2009.
- [7] Kano, J., Mio, H., Saito, F., Correlation of grinding rate of gibbsite with impact energy of balls. *AIChE J.*, 46, 1694–1697, 2000.
- [8] Mishra, B.K., A review of computer simulation of tumbling mills by the discrete element method Part II - Practical applications, *Int. J. of Min. Processing*, 71, 95-112, 2003.
- [9] Jayasundara C.T, Yang R.Y, Yu A.B, Curry D., Discrete particle simulation of particle flow in IsaMill, *Industrial and Engineering Chemistry Research*, 45:6349-6359, 2006.
- [10] Jayasundara, C.T., Yang, R.Y., Yu, A.B., Rubenstein, J., Effects of disc rotation speed and media loading on particle flow and grinding performance in a horizontal stirred mill, *International Journal of Minerals Processing*, 9627-35, 2010.
- [11] Prasher, C. L. *Crushing and Grinding Process Handbook*, Wiley: Chichester, U.K., 1987.
- [12] Wills, B. A., *Mineral Processing Technology*, 5th Edition; Pergamon Press: Oxford, U.K., 1992.
- [13] Mindlin, R.D., Deresiewicz, H., Elastic spheres in contact under varying oblique forces, *Journal of Applied Mechanics* , 20, 327-344, 1953.
- [14] Rajamani, R. K., Mishra, B. K., Venugopal, R., and Datta, A., Discrete element analysis of tumbling mills, *Powder Technology*, 109, 105, 2000.
- [15] Schubert, W., Khanal, M., Tomas, J., Impact crushing of particle–particle compounds— experiment and simulation, *International Journal of Mineral Processing*, 75, 41– 52, 2005.
- [16] Thompson, P. A., and Grest, G. S., Granular flow: friction and the dilatancy transition, *Physical Review Letters*, 67, 1751, 1991.
- [17] Yuu, S., Abe, T., Saitoh, T., and Umekage, T., Three-dimensional numerical simulation of the motion of particles discharging from a rectangular hopper using distinct element method and comparison with experimental data (effects of time steps and material properties), *Advanced Powder Technology*, 4, 259, 1995.
- [18] Zhang, Y., Campbell, C. S., The interface between fluid-like and solid-like behaviour in two-dimensional granular flows, *Journal of Fluid Mechanics*, 237, 541, 1992.
- [19] Zhu, H.P., Zhou, Z.Y., Yang, R.Y., Yu, A.B., Discrete particle simulation of particulate systems: Theoretical developments, *Chemical Engineering Science*, 62, 3378-3396, 2000.